Novel Pd/GdCrO$_3$ composite for photo-catalytic reduction of nitrate to N$_2$ with high selectivity and activity

Zhiang Hou[a], Fangfei Chen[a], Jinnan Wang[a,*], Corvini Philippe François-Xavier[b], Thomas Wintgens[b]

[a] State Key Laboratory of Pollution Control and Resource Reuse & School of the Environment Nanjing University, Nanjing, 210023, China
[b] School of Life Sciences, University of Applied Sciences and Arts Northwestern Switzerland, Basel, 4132, Switzerland

ABSTRACT

Although photocatalytic reduction of nitrate attracted much attention recently, undesired intermediate products (nitrite and ammonium) limited its application in practice. In this study, novel Pd/GdCrO$_3$ composite was successfully synthesized to photo-catalytically reduce nitrate to N$_2$ with high selectivity. Compared with TiO$_2$ (P25), GdCrO$_3$, Ag/GdCrO$_3$ and Cu/GdCrO$_3$, 1 wt% Pd/GdCrO$_3$ achieved higher removal rate of nitrate (98.7%) and selectivity to N$_2$ (100%). The kinetics constant of 1 wt% Pd/GdCrO$_3$ was two times higher than that of P25. Even after six cycling runs, 1 wt% Pd/GdCrO$_3$ still remained high photocatalytic reduction rate of nitrate (95.5%) and selectivity to N$_2$ (98.4%). Such advantages were not only attributed to the negative conduction band value of GdCrO$_3$ but also attributed to the co-catalyst effect of Pd. On one hand, nano particles Pd improved the utilization of charge carriers of GdCrO$_3$. On the other hand, nitrite was easily reduced to NO* on nano particles Pd surface, followed by decomposition step to N* and O*, and then the reduction of nitrite in the vicinity of the N* could yield N$_2$O* which would be preferentially transformed into N$_2$. Accordingly, high concentration of nitrite accumulated initially could enhance the likelihood of N* encountering nitrite so as to increasing the N$_2$ selectivity. In addition, electron paramagnetic resonance and hole scavenger experiments demonstrated that both photo-generated electrons and CO$_2\cdot-$ played important role in photocatalytic reduction process, suggesting a different mechanism from P25 where nitrate was mainly reduced by CO$_2\cdot-$. Thus, the present work not only prepared a promising photocatalyst for reduction of nitrate in water/wastewater treatment process, but also provided a simple and efficient way to improve the photocatalytic activity and selectivity to N$_2$ of photocatalysts.

1. Introduction

Nitrate contamination of groundwater and surface water, mainly resulting from intensive agricultural activities using nitrogen fertilizers, has become a widespread problem throughout the world [1,2]. High nitrate levels have a latent huge damage to human health because nitrate could be reduced to nitrite in the human body, which could cause various diseases such as methemoglobinemia, "blue baby" syndrome, even cancers [3]. Considering that, the World Health Organization has limited the concentration of NO – 3below 50 mg L^{-1}.

Photocatalytic reduction of nitrate into nitrogen over semiconductor materials is a relatively new technique, but it has shown high efficacy and great potential for nitrate removal. Photocatalytic decomposition of nitrate using TiO$_2$ was firstly reported by Robert Schlögl in 1999 [4]. Since then, as a simple and efficient technology,

photocatalytic reduction of nitrate was extensively investigated by researchers. Due to its high level of photocatalytic activity, optical-electronic properties, high photostability, low cost and non-toxicity [5–8], titanium oxide (TiO$_2$) has been considered as one of the most promising photocatalysts for its application for hydrogen generation [7,9–11] and degradation of organic pollutants [12–17]. Thus, most of researchers focused on the investigation of TiO$_2$ based materials for photocatalytic reduction of nitrate (Table 1).

However, selection of a photocatalyst to catalyze a particular reaction depends on the relative position of the conduction and valence bands of the photocatalyst with respect to the redox potentials for the desired reactions. The chemical potentials of photo-generated electrons and holes depend on the position of the energy levels in the semiconductor. More specifically, the redox potential of a donor species adsorbed on the surface of the photocatalyst needs to be more negative

Table 1
Photoreduction of nitrate over TiO2-based photocatalysts in previous literatures.

Photocatalysts	$[NO-3]_0$ (mMol)	Hole scavenger	Conversion (%)	Reaction time/(min)	Selectivity (%)			Reference
					$NO-2$	$NH+4$	N_2	
TiO_2(P25)	7.1	Formic acid	15.2	30	0	0	100	[18]
TiO_2(P25)	7.1	Formic acid	99	180	0	42	58	[19]
TiO_2 (Hombikat)	7.1	Formic acid	100	180	0	45	55	[19]
TiO_2(P25)	0.8	Formic acid	52.5	120	23	6	38.1	[20]
TiO_2	1.0	Benzene	8	240	0	56.8	43.2	[21]
TiO_2(P25)	0.25	bio-electrons from microbial metabolism	60	1440	0	4	96	[22]
Cu/ TiO_2(P25)	0.7	Glycerol	98	120	0	2	98	[23]
Cu/ TiO_2(P25)	0.7	Formic acid	100	180	0	37-60	40-63	[19]
Cu/ TiO_2	0.6	Formic acid	93.73	120			0	[24]
Cu_2O/TiO_2(P25)	1.6	Oxalic acid	57.6	180	12.4	45.7	41.9	[25]
Fe/ TiO_2(P25)	0.7	Formic acid	100	180	0	23	77	[19]
Pt/TiO_2 + SnPd/Al_2O_3	1.0	Glucose	23	720	3	22	75	[26]
Pt/TiO_2(P25)	10	Oxalic acid	6.4	180	1.2	31.3	67.5	[27]
Pd/TiO2(P25)	10	Oxalic acid	2.6	180	3.1	76.9	20	[27]
Pd/TiO2(P25)	10	Oxalic acid	6.0	720	0	0	0	[28]
Au/TiO_2	1.6	Oxalic acid	34-60	180				[29]
Au/TiO_2	1.6	Oxalic acid	44	180	0	39	61	[30]
Ag/TiO2(P25)	7.1	Formic acid	71.7	30	11.5	0.167	83.7	[18]
Ag/TiO2(P25)	7.1	Formic acid	100	180	0	4	96	[19]
Ag/TiO2(P25)	7.1	Formic acid	99.6	240	2.3	9.3	88.4	[31]
Ag_2O/ TiO_2(P25)	7.1	Formic acid	51.9-97.5	240	0.3-44.6	0.7-14.0	12.7-85.3	[31]
Pt-Cu/TiO_2	1.0	Benzene	63.3	240	1	1	90	[21]
Pd-Cu/TiO_2(P25)	1.6	CO_2 + H_2 + Humic acid	100	240	0	< 2	> 98	[32]
Pd-Cu/TiO_2(P25)	0.8	H_2 + Formic acid	39-100	60	0	0-13.7	86.3-100	[33]
Sn–Pd/TiO_2(P25)	10	Ethanol	19	240	0	23	77	[34]
Sn–Pd/Pt/TiO_2(P25)	10	Ethanol	23	240	0	24	76	[34]

(higher in energy) than the valence band position of the semiconductor in order to replenish the electron vacancies. For TiO_2, low reduction potential ($E_{CBM} = -0.5$ V) and high oxidation potential ($E_{VBM} = 2.7$ V) (all the potentials were reported versus standard hydrogen electrode, NHE; pH = 7) [35], makes TiO_2 a mildly reducing and strong oxidizing photocatalyst [36]. Although it is possible for TiO_2 photocatalytic reduction of NO – 3according to the thermodynamic theory [E°(NO – 3/ NO – 2) = 0.49 V; E°(NO – 3/N_2) = 1.25 V; E° (NO – 3/ NH+ 4) = 1.203 V], the photocatalytic reduction of nitrate over TiO_2 is inefficiency because of its relative weak reducibility. In addition, due to high E_{VBM} of TiO_2, easy formation of •OH radicals may reoxidize nitrite or ammonium to nitrate [20]. Consequently, undesired byproducts (nitrite and ammonium) are produced which lead to the low selectivity of N_2. In order to improve the conversion rate and selectivity to N_2, various metals (Pt, Pd, Fe, Cu, Au, Ag) was loaded on TiO_2 [18,19,26,29,37]. For instance, Ag (0) loaded on TiO_2 can form Schottky barrier so as to not only promoting the separation of photogenerated electron-hole pairs on the bulk TiO_2 but also enhancing the separation time of electrons and holes. Thus, Ag/TiO_2 showed high photocatalytic selectivity (nearly 100%) to N_2, and one order of magnitude higher activity than the hydrogenation catalysts [18]. However, further studies indicated that the photocatalytic stability of Ag/TiO_2 was poor because its catalytic ability decreased significantly in the second cycle, and new catalysts with a good reusability in the reduction of nitrate still remain to be developed [31]. Other photocatalysts such as CdS [38,39], ZnS [40], $SrTiO_3$ [41], were also investigated for photocatalytic reduction of nitrate. However, their conversion rate and selectivity to N_2 were still unsatisfied.

In recent years, much attention was paid to rare earth orthochromites ($RCrO_3$) due to their unique physical properties which arise from the orthorhombically distorted perovskite structure [42]. For rare earth elements, the energy level of 4f orbit is higher than that of 5S and 5p orbits, and the 4f electronic shell is in the inner orbit. Thus, 4f electronic shell is insusceptible under the shelter of outer electronic shells and orbits [43]. More importantly, since $RCrO_3$ have rich energy levels, large number of transitional electrons and the interaction between rare earth elements and transition elements, various attempts were made to

apply $RCrO_3$ as catalyst for reduction of SO_2 and purification of automobile exhaust. As a typical $RCrO_3$, $GdCrO_3$ (Eg = 2.7 eV)[44] was tried for photocatalytic spitting water to produce hydrogen due to its negative conduction band value (−2.02 V) (Fig. S1). From thermodynamic point of view, if the conduction band value of catalyst is negative enough, it would be expected to directly electron-drive catalytic reduction of nitrate by $GdCrO_3$.

On the other hand, catalytic hydrogenation of nitrate by bimetallic catalysts [noble metals (Pt, Pd and Rh) and secondary metals (Cu, Sn and In)] was reported in many literatures [45–49]. As the most active and selective combination of Pd-Cu, Cu is responsible for the conversion of NO − 3 into NO − 2, while Pd subsequently converts NO − 2 into N_2 and NH+ 4[48] (Eqs. (1)–(3)). Thus, we have reason to believe that these conversion processes can occur during the photocatalytic reduction of nitrate. Based on this assumption, we supposed that $GdCrO_3$ loaded of noble metal could efficiently improve the selectivity to N_2. In addition, it was reported that the presence of noble metals (Pd, Ag, Pt) in photocatalytic systems could reduce the recombination of photogenerated electrons/holes and prolong the charge-carrier lifetime [50,51]. Therefore, once photo-generated electrons were transferred from the conduction band of $GdCrO_3$ to loaded noble metals, the photogenerated electrons are more conductive to photoreduction of nitrate.

$$NO_3^- + H_2 \xrightarrow{Pd-M} NO_2^- + H_2O \tag{1}$$

$$2NO_2^- + 3H_2 \xrightarrow{Pd} N_2 + 2H_2O + 2OH^- \tag{2}$$

$$NO_2^- + 3H_2 \xrightarrow{Pd} NH_4^+ + 2OH^- \tag{3}$$

Herein, we report for the first time the photocatalytic reduction of nitrate with high selectivity of N_2 by Pd/$GdCrO_3$. Being attributed to the negative conduction band value of $GdCrO_3$, it is expected that nitrate could be reduced to N_2 not only by $CO_2 \cdot -$ radicals but also by photo-generated electrons, suggesting a different mechanism from P25 where nitrate was mainly reduced by $CO_2 \cdot -$ radicals. More importantly, co-catalyst of nano particles Pd could not only accelerates separation of electron-hole pairs to improve the photocatalytic activity,

but also significantly improve the conversion rate of NO – 2 into N$_2$. In summary, the present work not only prepares a promising photocatalyst for removal of nitrate from water/wastewater, but also provides a efficient way to enhance the selectivity to N$_2$ in the process of photocatalytic reduction of nitrate. To achieve this goal, our study focused on the following three aspects: 1) to synthesize and characterize novel photocatalyst Pd/GdCrO$_3$, 2) to evaluate the photocatalytic activity and selectivity to N$_2$ over Pd/GdCrO$_3$, and 3) to illustrate the different mechanisms involved in the photocatalytic reduction of nitrate over Pd/GdCrO$_3$, GdCrO$_3$ and (P25).

2. Experimental

2.1. Chemicals

In this study, TiO$_2$ used as comparison was commercially available Degussa P25 (Germany) with a surface area of ca. 50 m^2 g^{-1}, consisted of two phases of anatase (80%) and rutile (20%). All reagents were of analytical grade and used without further purification.

2.2. Preparation of catalysts

2.2.1. Synthesis of GdCrO$_3$

GdCrO$_3$ was synthesized by solid state combustion method [44]. In detail, 0.451 g Gd(NO$_3$)$_3$·6H$_2$O, 0.076 g Cr$_2$O$_3$ and 0.24 g urea were mechanically mixed in an alundum crucible. In the presence of ethanol, the mixture was calcined at 800 °C for 4 h with a heating rate of 6 °C min^{-1}. Then the green and porous agglomerate was obtained and ground into powder in an agate mortar without further treatment.

2.2.2. Synthesis of Pd/GdCrO$_3$ and Pd/P25

0.2 g GdCrO$_3$ was added into the mixture including different amounts of 0.5 g L^{-1} PdCl$_2$ solution and 0.2 mol L^{-1} formic acid. Then the suspension was diluted with deionized water to 200 ml. After irradiated by a 500 w high-pressure Hg lamp for 40 minutes, the as-synthesized product was collected by centrifugation, and washed with distilled water for three times. Finally, the precipitate was dried at 60 °C for 10 h. In this manner, different weight ratios of the Pd to GdCrO$_3$ samples (i.e., 0.5 wt%, 1 wt%, 2 wt% Pd/GdCrO$_3$) were obtained. Furthermore, 1 wt%Pd/P25 was prepared by the same method.

2.2.3. Synthesis of Cu/GdCrO$_3$ and Ag/GdCrO$_3$

in order to comparatively study the influence of different metals loaded on GdCrO$_3$ upon photocatalytic performance, Ag/GdCrO$_3$ and Cu/GdCrO$_3$ samples were prepared by the same procedures except that AgNO$_3$ or CuSO$_4$·5H$_2$O was used instead of PdCl$_2$.

2.3. Characterization of catalysts

The morphology and microstructure of the samples were characterized using QUANTA FEG 250 scanning electron microscope (SEM). The composition of samples was determined with an energy dispersive X-ray spectroscopy (EDS) attached to scanning electron microscopy (SEM). To further observe the distribution of the nanoparticles of metals (Pd, Ag, Cu) loaded on GdCrO$_3$, transmission electron microscope (JEM-200CX, JEOL, Japan) analyses of different catalysts was conducted. The XRD patterns were obtained on an X-ray diffractometer (XRD, X'TRA, Switzerland) using Cu-kα radiation at a scan rate of 5°min^{-1} in the range of 10–80° (2θ). Surface chemical analysis was performed by X-ray photoelectron spectroscopy (XPS, PHI 5000 Versa Probe, ULVAC-PHI, Japan) with an Al- kα X-ray source. All the binding energies were referenced to the C 1 s peak at 284.8 eV of the surface adventitious carbon. The transient photocurrent responses were measured by the electrochemical workstation (CHI660E, Shanghai, China) with a conventional three-electrode system. The photoluminescence (PL) spectra were detected using Fluorescence spectrometry (Horiba HJY FM4P-TCSPC). Electron paramagnetic resonance (EPR) spectra were recorded on an EMX-10/12 (Bruker, Germany) with a 100 W high-pressure Hg lamp at room temperature. Moreover, 5, 5-dimeyhyl-1-pyrroline-*N*-oxide (DMPO) was used as the spin trap.

2.4. Photocatalytic tests

Photocatalytic reduction of nitrate was performed in the XPA-VII photocatalytic reactor (Xujiang Electromechanical Plant, Nanjing, China). A 500 w high pressure Hg lamp (main wavelength around 365 nm) placed axially at the center of the quartz immersion well was employed as the light source. Before initiating the reaction, 25 mg of catalyst and 50 ml of nitrate solution (50 mg L^{-1}) was added into the quartz tube (inner diameter = 2 cm, volume = 60 mL) and stirred for 30 minutes. Then 1 ml of formic acid (0.2 mol L^{-1}) as the hole scavenger was added in the mixture. The continuous circulation of cool water bath kept the temperature of the inside reactor at 25 ± 1 °C. During the irradiation, the samples were withdrawn periodically, and the catalysts were removed by filtration through 0.22 μm cellulose acetate membrane. The species of nitrogen (NO – 3, NO – 2) were determined using the ion chromatography (DIONEX ICS-1100). The concentration of NH + 4 was measured by using standard Nessler's reagent colorimetric method. Many literatures reported that the main reduction products were NO – 2, NH + 4 and N$_2$ in the photocatalytic denitrification [19,52], and N$_2$ selectivity could be calculated as Eq. (4).

$$S(N_2) = \frac{[NO_3^-]_0 - [NO_3^-]_t - [NO_2^-]_t - [NH_4^+]_t}{[NO_3^-]_0 - [NO_3^-]_t} \tag{4}$$

where S(N$_2$) is the N$_2$ selectivity, [X]$_0$ and [X]$_t$ are concentrations of nitrogen species at time 0 and t respectively.

3. Results and discussion

3.1. Characterization of photocatalysts

XRD spectra was used to analysis the purity and crystalline development of GdCrO$_3$ and GdCrO$_3$ decorated with various content Pd. All the diffraction peaks of the as-synthesized GdCrO$_3$ (Fig.1a) are well matched with the pure GdCrO$_3$ (JCPDS Card No. 25-1056). However, the diffraction peaks of Pd could hardly be found from the XRD patterns, which may be attributed to its poor crystallinity or low content of very small Pd nanoparticles. The GdCrO$_3$ crystallizes in a distorted perovskite type structure with four formula units per unit cell where each Cr was surrounded by six oxygen atoms forming CrO$_6$ octahedral geometry (Fig. 1b). And the distortion is due to the mismatch of Gd–O and Cr–O bond lengths [53]. The distorted perovskite structures have greater influences on the photocatalytic performance than orthogonal and cubic crystal structures.

XPS analysis was used to further identify the existence of Pd and the chemical state of the 1 wt% Pd/GdCrO$_3$ composites. Fig. 2a represents the survey scan spectra of 1 wt% Pd/GdCrO$_3$ composite. XPS scan signals originating from Gd 4d, C 1 s, Pd 3d, O 1 s, and Cr 2p, are easily identified at binding energies around 142.4 eV, 284.8 eV, 336.2 eV, 530.2 eV and 576.2 eV, respectively. The intense peak of Gd^{3+} 4d$_{3/2}$ and 4d$_{5/2}$ levels were located at 147.1 and 142.4 eV, respectively (Fig. 2b). The peaks at binding energies 576.2 and 586.3 eV are associated to the Cr^{3+} 2p$_{3/2}$ and Cr^{3+} 2p$_{1/2}$ levels, respectively (Fig. 2c). In Fig. 2d, the binding energies around 335.2 and 340.5 eV are corresponding to Pd 3d$_{5/2}$ and 3d$_{3/2}$ levels which indicated that metallic Pd were successfully attached on GdCrO$_3$.

SEM images (Fig. 3a) and TEM images (Fig. 3b) indicate that the GdCrO$_3$ powders are sheet particles with irregular appearance. In addition, TEM images (Fig. 3c) show that the Pd nanoparticles (average diameter of 5.7 nm) (Fig. 3d) well dispersed on the surface of Pd/GdCrO$_3$ composites. The uniform distribution of Pd nanoparticles was
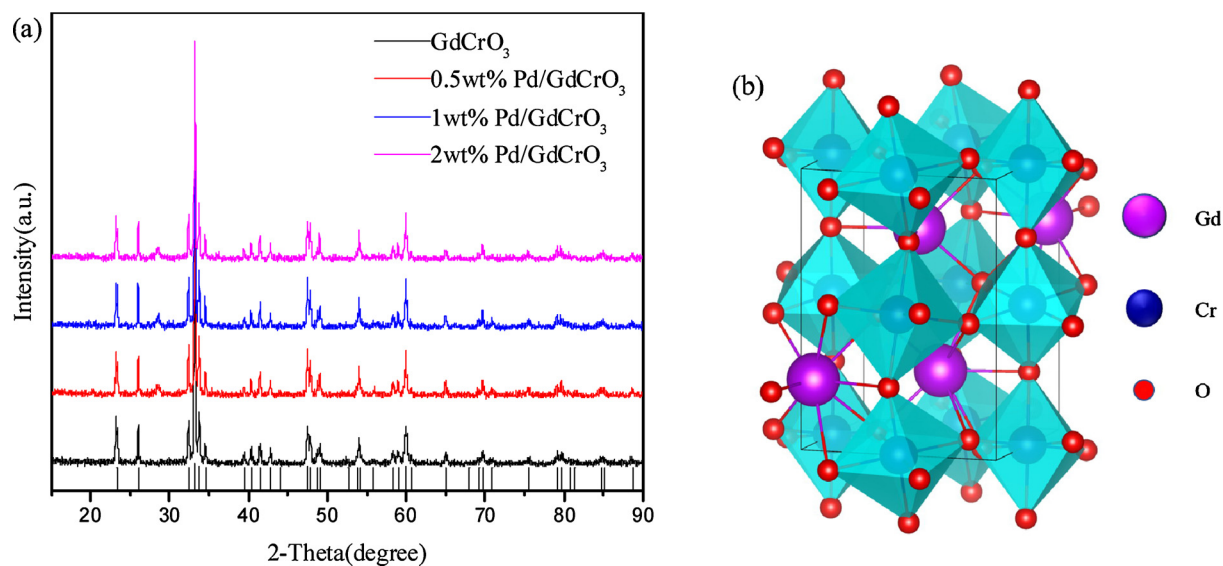
Fig. 1. (a) XRD patterns of catalysts, (b) Schematic representation of distorted perovskite structure of GdCrO₃.
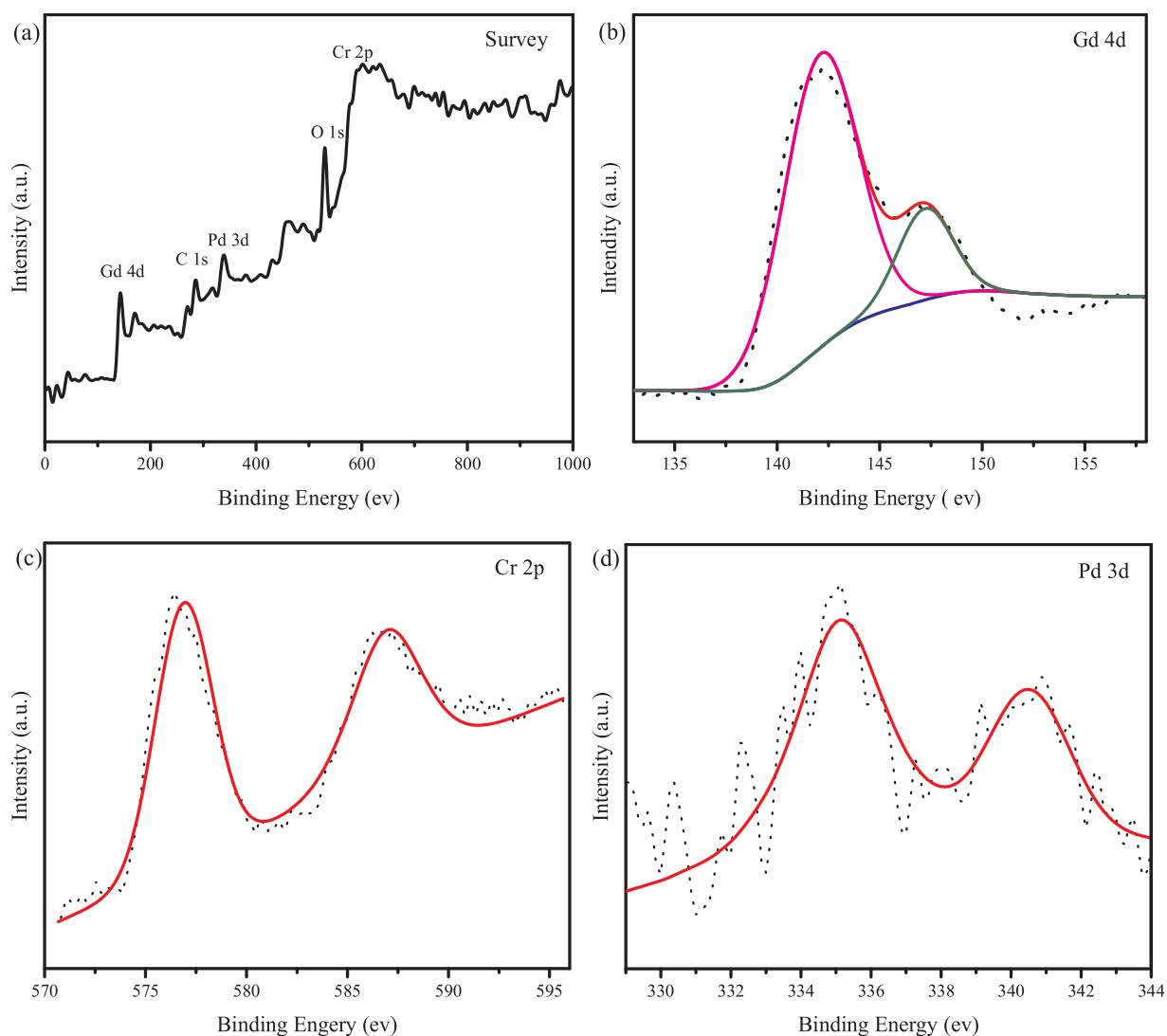

Fig. 2. XPS spectra of 1 wt% Pd/GdCrO₃. (a) Survey, (b) Gd 4d, (c) Cr 2p, (d) Pd 3d.

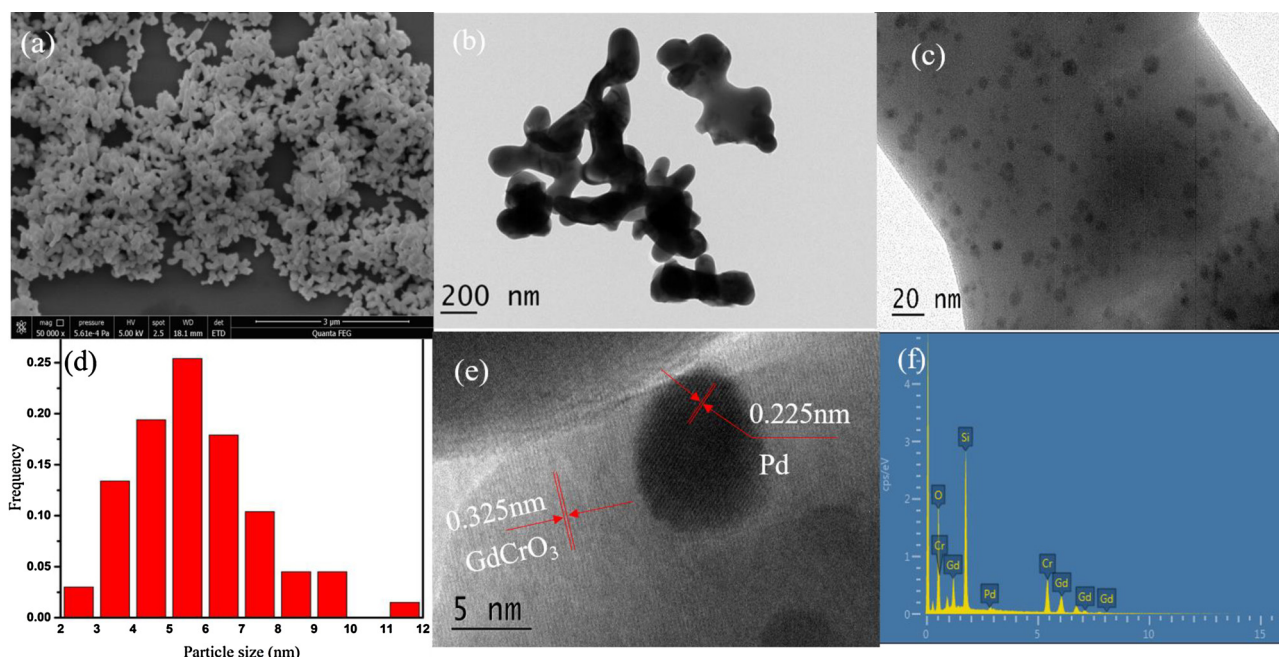**Fig. 3.** (a) The SEM image of GdCrO₃, (b) the TEM image of GdCrO₃, (c) TEM image of 1 wt%Pd/GdCrO₃, (d)particle distribution of Pd, (e) HRTEM image of 1 wt%Pd/GdCrO₃, (f) EDS spectrum of 1 wt%Pd/GdCrO₃.

beneficial to enhancing the photocatalytic performance. High-resolution TEM image (HRTEM) further confirms that the Pd nanoparticles are successfully loaded on Pd/GdCrO₃. The lattice fringes of Pd and GdCrO₃ could be clearly observed in the composite of 1 wt%Pd/GdCrO₃ (Fig. 3e). Fig. 3f shows the energy dispersive X-ray spectrometry (EDS) of Pd/GdCrO₃ composites. It should be noted that Pd, Gd, Cr and O peaks were from Pd/GdCrO₃, while Si peaks were from the Silicon substrate.

3.2. Photocatalytic reduction of nitrate over Pd/GdCrO₃

When 0.8 mmol L^{-1} NO – 3 and 1.0 mmol L^{-1} FA were mixed in the absence of the photocatalyst, there was no observation of NO – 3 reduction under both dark and irradiation conditions, which excluded the possibility of a direct redox reaction between NO – 3 and FA. The photocatalytic activities of various catalysts follow the order of 1 wt% Pd/GdCrO₃ > 0.5 wt% Pd/GdCrO₃ > 2 wt% Pd/GdCrO₃ > 1 wt% Pd/P25 > GdCrO₃ > P25. The 1 wt% Pd/GdCrO₃ composite material shows the highest photocatalytic activity, which demonstrated that Pd significantly improved the photocatalytic performance of GdCrO₃. However, further increasing the content of Pd nanoparticles led to decrease of photoactivity, which might be ascribed to the fact that high content of Pd nanoparticles could act as charge carrier recombination centers and thus resulted in a decrease of photocatalytic activity. Such phenomenon was also observed in previous studies when using noble metal nanoparticles as the electron reservoir [54,55]. Meanwhile, the photocatalytic reduction kinetic curves of NO – 3 over various catalysts can be well described by the first-order kinetics equation (Fig.4b). The 1 wt% Pd/GdCrO₃ exhibits the highest photocatalytic rate constant which was about 3 and 1.5 times higher than that of P25 and pure GdCrO₃, respectively.

Generally, nitrate could be reduced to N₂, NO – 2and NH+ 4. Since NH+ 4 and NO – 2 were still considered as the pollutants in environment, improvement of selection of N₂ was more important than reduction rate of nitrate. In the presence of formic acid (FA) serving as the hole scavenger, nitrate reduction and the distribution of products over P25, 1 wt%Pd/P25, GdCrO₃ and 1 wt% Pd/GdCrO₃ are shown in Fig. 5(a–d). The concentration of NO – 2 firstly increased at 20 min over these three photocatalysts. The accumulated NO – 2 at 20 min

decreased slowly and finally reduced to 0.094 mmol L-1 (11.6%), while the concentration of NH+ 4 was constantly increased to 0.051 mmol L^{-1} (6%) at 100 min, which exhibited 72.8% NO – 3 conversion rate and 75.7% selectivity to N₂ over P25 (Fig. 5a). Generally, P25 consists of anatase (80%) and rutile (20%). It was determined that the CB of anatase lies 0.2 eV above the CB of rutile [56], with rutile having Eg of 3.03 eV and anatase having Eg of 3.2 eV. These energetics favored charge carrier separation upon irradiation in a way that electrons were transferred to the rutile CB, and the holes to the VB of anatase. Thus, multiphase heterojunctions of P25 contributed to the efficient carrier separation, which made P25 showed more than 70% conversion rate of NO – 3. As for 1 wt%Pd/P25, the loading of Pd improved the conversion rate of NO – 3 (Fig.5b).However, the selectivity of N₂ was still low (86.2%) because that high E_{VBM} of TiO₂ could lead to generating ·OH radicals which might reoxidize nitrite or ammonium to nitrate [20].

On the other hand, although there were no multiphase heterojunctions in the GdCrO₃ crystal, GdCrO3 still show slight higher reduction efficiency of nitrate and selectivity to N₂ than P25 because of its strong reduction ability (Fig.5c). The concentration of NH+ 4 was first increased and finally decreased to 0.023 mmol L^{-1} (2.8%), which showed that the accumulated NO – 2 still could not be completely removed in the system of pure GdCrO₃. Compared with P25, 1 wt%Pd/ GdCrO₃ exhibits higher removal rate of NO – 3 (98.7%) and selectivity of N₂ (100%) (Fig.5d). Not only NH+ 4 was always maintained at a low level (even close to 0), but also the accumulated NO – 2 was almost decreased to 0 after100 min over Pd/GdCrO₃. The conduction band value of GdCrO₃ was calculated in Fig. S1, the possible exists of oxygen vacancies have no obvious effect on the energy band positions [57,58]. Thus, such advantages might be explained as follows: 1) the negative conduction band value of GdCrO₃ (− 2.02 V) is beneficial to photocatalytical reduction, 2) with high conductivity and catalytic activity, Pd could not only prevent the recombination of electron-hole pairs but also induce faster electrons migration from CB of GdCrO₃ to Pd. Such mechanism would be further discussed in Section 3.3.

In addition, as an important factor to evaluate the catalysts performance, the stability of catalysts should be taken into consideration in the practical application. 1 wt%Pd/GdCrO₃ could maintain high nitrate conversion rate and N₂ selectivity even after 6th cycle. Only 3.2%
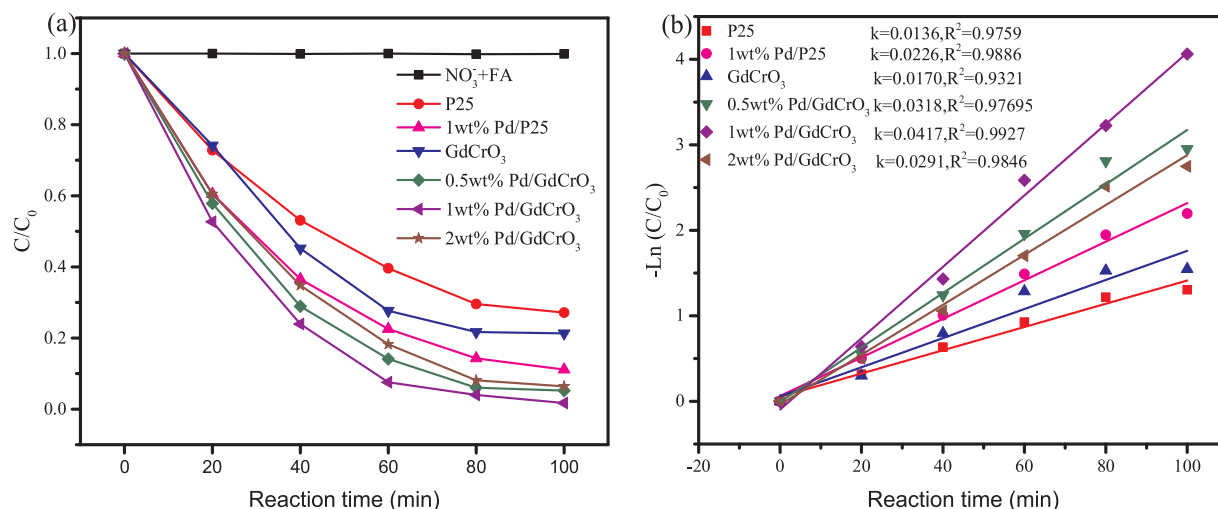
Fig. 4. (a) Photocatalytic reduction of nitrate over different photocatalysts, (b) kinetic fit for the photocatalytic reduction of nitrate with different photocatalysts.

decrease of nitrate conversion rate was observed and this slight decrease was probably due to the loss of catalyst during the repeated experiments (Fig. 5e). Furthermore, the leaching of Cr during the reaction process are lower than the limitation of WHO (< 0.05 ppm) (Fig. S2). Subsequently, we also analyzed the 1 wt% Pd/GdCrO$_3$ by XPS spectra (Fig. 5f) and XRD patterns (Fig. 5g) before and after photocatalytic reduction of NO – 3. The Pd 3d$_{5/2}$ and Pd 3d$_{3/2}$ peaks of Pd, do not shift obviously, which demonstrated that there were no valence changes of Pd after six cycling photocatalytic reduction. Moreover, XRD patterns of 1 wt% Pd/GdCrO$_3$ after 6 times cycles confirmed the structural stability of this catalyst. Being attributed to high nitrate conversion rate, N$_2$ selectivity and catalytic stability, 1 wt% Pd/GdCrO$_3$ could be a promising photocatalyst for the reduction of nitrate in the environmental protection.

3.3. Co-catalytic effect of Pd

Generally, photocatalytic reaction involved three basic steps: (1) photocatalysts absorbed photons with sufficient energy so as to induce electrons to transfer from the VB to the CB and leaving an equal number of holes; (2) the photo-generated electron-hole pairs separated and migrated to the surface of photocatalysts; and (3) they oxidized the electron donors and reduced electron acceptors which were absorbed on the catalyst surface, respectively [59]. However, recombination of photo-generated electrons-holes could significantly reduce the photocatalytic efficiency in step (2) [60]. The loading of Pd on the surface of GdCrO$_3$ was beneficial to preventing the recombination of electron-hole pairs, which could be explained as follows: (1) the formation of heterojunctions between Pd and GdCrO$_3$ provided an internal electric field which could facilitate separation of the electron-hole pairs; and (2) Pd could provide strong electron-sink effect so as to inducing faster electrons migration from CB of GdCrO$_3$ to Pd. The photocurrent versus the irradiation time (I–t) curves and Photoluminescence (PL) spectra of pure GdCrO$_3$ and 1 wt% Pd/ GdCrO$_3$ could well confirm the explanation mentioned above. The 1 wt% Pd/GdCrO$_3$ produced much stronger photocurrent intensity (about 3 times higher) than pure GdCrO$_3$ (Fig. 6a), which reflected the higher separation efficiency of photoexcited electron-hole pairs of 1 wt% Pd/GdCrO$_3$. In addition to transient photocurrent experiments, the PL technique was considered as an effective means of investigating the separation efficiency of electron-hole pairs in a photocatalyst. Pure GdCrO$_3$ exhibited strong emission from 400 to 550 nm excited at 240 nm, while the PL peak was weaken significantly after the addition of Pd (Fig. 6 b). Such difference indicated that efficient interfacial electrons transferred from the conduction band of GdCrO$_3$ to Pd nanoparticles, which act as electron sinks

and hamper the recombination of photo-generated carriers. This result strongly agreed with the transient photocurrent experiments. On the other hand, since Pd itself exhibited high catalytic activity and electron conductivity, Pd-based catalytic reduction held great promise for the removal of NO – 3 and NO – 2 from water [61,62].

Notably, loading Pd on GdCrO$_3$ could not only significantly enhance NO – 3 removal but also enhance N$_2$ selectivity. As the most used co-catalysts in the nitrate photocatalytic reduction system, Ag and Cu are also decorated on the GdCrO$_3$ for comparative study (Table 2). Although NH + 4 maintained at a low level under Ag/GdCrO$_3$ and Cu/GdCrO$_3$, modification of Ag and Cu on GdCrO$_3$ could not obviously enhance the removal rate of NO – 3. Meanwhile, accumulation of NO – 2 was observed obviously by 1 wt% Ag/GdCrO$_3$ and 1 wt% Cu/GdCrO$_3$, which indicated that the conversion from NO – 2 to N$_2$ was relatively low. Thus, compared with Cu and Ag, Pd could play more important role in enhancement of N$_2$ selectivity. The density functional theory (DFT) calculation suggested that N$_2$ selectivity was determined at the nitrite reduction step on the Pd surface. NO – 2 was easily reduced to NO* on the Pd surface, followed by either sequential hydrogenation steps to yield NH$_3$ or a decomposition step to N* and O* (an adsorbate on Pd is denoted using an asterisk) [63]. It suggested that the reduction of NO – 2 in the vicinity of the N* could yield N$_2$O* which would be preferentially transformed into N$_2$. Accordingly, high concentration of NO – 2 was beneficial to enhancing the likelihood of N* encountering NO – 2 in the solution phase which was important for maximizing the N$_2$ selectivity. Therefore, the NO – 2 accumulated in the initial 20 min, and then reduced to N$_2$ effectively on the surface of co-catalyst of Pd.

3.4. Photocatalytic mechanism

Generally, in the system of TiO$_2$, the strong reductive CO$_2$· − radicals [E° (CO$_2$/CO$_2$· −) = − 1.8 V] [64] produced by the oxidation reaction between the photo-generated holes and formic acid plays a dominate role for the photocatalytic reduction of nitrate and nitrite [18–20]. In addition, K. Doudrick et al. proposed that the photo-generated electrons could also be used to photocatalytic reduction of nitrate and nitrite [52]. To investigate the photocatalytic reduction process, electron paramagnetic resonance (EPR) and hole scavenger experiments were conducted. No EPR signals are found in dark conditions. Four-line EPR signals with intensity ratios of 1:2:2:1 representing ·OH were observed in the system of P25 + H$_2$O under UV irradiation (Fig. 7a), demonstrating that P25 could oxide H$_2$O to produce ·OH. Different from P25, there are no EPR signals of ·OH were observed in the system of GdCrO$_3$ + H$_2$O under UV irradiation (Fig. 7 b), indicating that GdCrO$_3$ could not oxide H$_2$O to produce ·OH. In addition, EPR
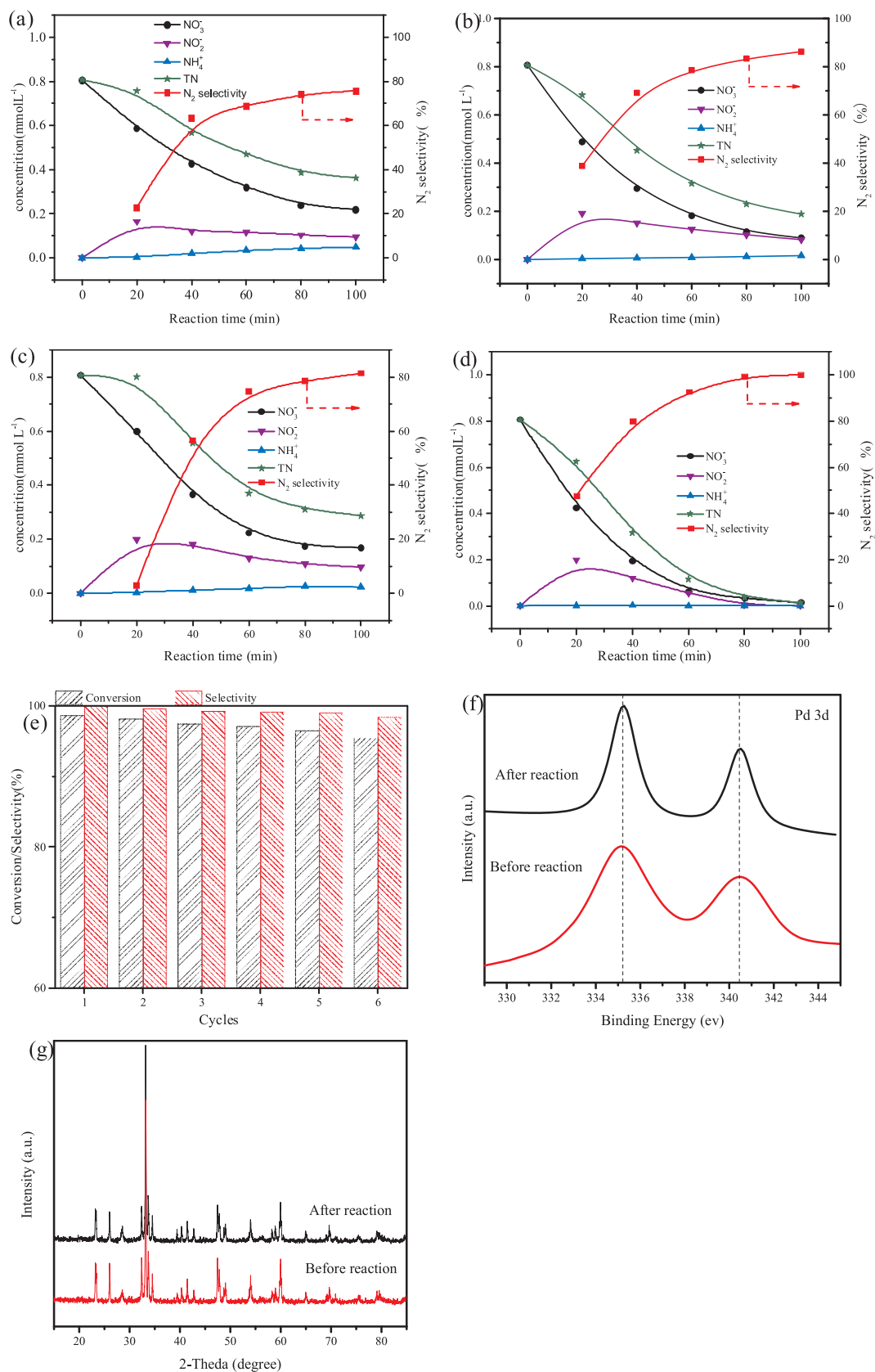
Fig. 5. Time course of NO – 3, NO – 2, NH+ 4 and N$_2$ selectivity during the process of photocatalytic denitrification (a) P25, (b) 1 wt% Pd/P25, (c)GdCrO$_3$, (d) 1 wt% Pd/GdCrO$_3$; (e) Cycling runs of 1 wt% Pd/GdCrO$_3$ for photocatalytic reduction of nitrate; (f) XPS spectra and (g) XRD patterns of 1 wt%Pd/GdCrO$_3$ before and after photocatalytic denitrification.

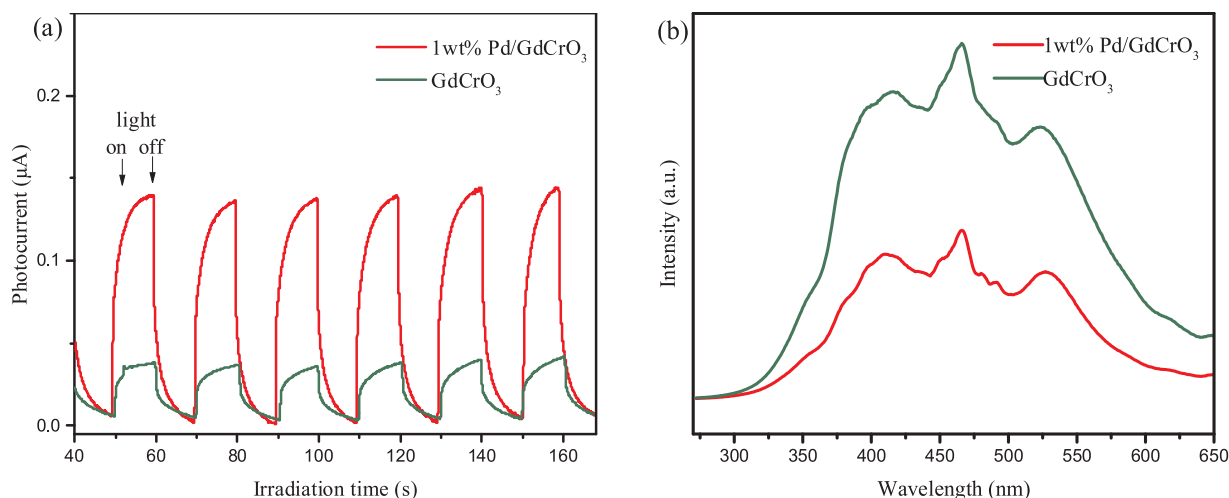**Fig. 6.** (a) Photocurrent response for $GdCrO_3$ and 1 wt%Pd/$GdCrO_3$; (b) Photoluminescence (PL) spectra of $GdCrO_3$ and 1 wt%Pd/$GdCrO_3$.
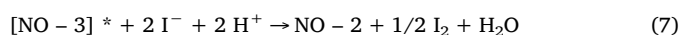
Table 2
Photocatalytic reduction of nitrate over different photocatalysts.[*]

Catalysts	Conversion of NO_3^- (%)	Yield of NO_2^- (%)	Yield of NH_4^+ (%)	Selectivity to N_2 (%)
P25	72.8	11.6	6	75.7
1 wt%Pd/P25	88.9	10.2	2.0	86.2
$GdCrO_3$	79.3	11.8	2.8	81.4
0.5 wt%Pd/ $GdCrO_3$	93.6	4.6	0	95
1 wt%Pd/ $GdCrO_3$	98.7	0	0	100
2 wt%Pd/ $GdCrO_3$	93	0.21	0.6	97.1
1 wt%Ag/ $GdCrO_3$	85.1	14	0.4	83.2
1 wt%Cu/ $GdCrO_3$	81.9	16.1	0.9	78.8

[*] Reaction conditions: $C_0[NO_3^-] = 0.8$ mmol L^{-1}; catalyst: 0.5 g/L; 0.4 mmol formic acid; reaction time: 100 mins.

signals with $a^N = 15.8$ G, a H β = 19.1 G, and g = 2.0058 are observed both in the system of (P25 + FA + NO_3^-) and ($GdCrO_3$ + FA + NO_3^-) under UV irradiation (Fig. 7a, b). Furthermore, loading Pd on $GdCrO_3$ does not change the EPR signals (Fig. 7 c). According to previous literatures report by Perissinotti et al, the EPR signals could directly confirm the existence of $CO_2 \cdot -$ [65]. Thus, $CO_2 \cdot -$ was involved in the photocatalytic denitrification process by P25, $GdCrO_3$ and1 wt% Pd/$GdCrO_3$. The stronger EPR signals of P25 might be due to the stronger oxidation ability of P25 ($E_{vbm} = 2.7$ V) than $GdCrO_3$ ($E_{vbm} = 0.68$ V). In considering that I^- could be oxidized to I_2 [E° (I_2/ I^-) = 0.536 V] without generation of $CO_2 \cdot -$, KI was used as the hole scavenger instead of formic acid in the hole scavenger experiment. However, we surprisingly found that the KI could reduce nitrate under UV irradiation without any photocatalysts. This might be explained by that nitrate photolysis would occur in water under UV irradiation (270–330 nm) with a maximum absorption at 300 nm. The first step in nitrate photolysis is the transition n → π* ($\varepsilon = 7.4$ M^{-1} cm^{-1}), which yielded unstable nitrate species ($[NO_3^-]$ *) in an excited state (Eq. (5)) [66]. $[NO_3^-]$ * could be decomposed without I- (Eq. (6)) or react with KI (Eq. (7)

$$NO_3^- + h\nu \rightarrow [NO_3^-]^* \tag{5}$$

$$[NO_3^-]^* \rightarrow NO_2^- + 1/2 \ O_2 \tag{6}$$

$$[NO_3^-]^* + 2 I^- + 2 H^+ \rightarrow NO_2^- + 1/2 \ I_2 + H_2O \tag{7}$$

Although NO_3^- is reduced by KI under UV irradiation in the absence of photocatalysts, the main products are NO_2^- and NH_4^+, showing low selectivity to N_2 (Fig. 7c). As for P25, due to the absence of reductive radicals, the conversion rate of NO_3^- and selectivity to N_2 respectively decreased 54% and 44.1% as KI was used as the hole scavenger. Thus, we suggested that photocatalytic reduction of nitrate by P25 mainly relies on $CO_2 \cdot -$ radicals, which was in agreement with previous literatures [19,20]. For $GdCrO_3$ and 1 wt%Pd/$GdCrO_3$ the conversion rate only respectively declined 16.7% and 12.2%, which could be explained by that the E_{CB} value (-2.02 V) of $GdCrO_3$ was negative enough for photo-generated electrons to directly reduce NO_3^- and NO_2^-. Notably, selectivity to N_2 of $GdCrO_3$ and 1 wt%Pd/ $GdCrO_3$ decreased 22.6% and 4.6%, respectively. It indicated that the decoration of Pd on $GdCrO_3$ could improve the selectivity to N_2 even in the absence of $CO_2 \cdot -$ radicals. Based on above test results, we suggested that $CO_2 \cdot -$ and photo-generated electrons at the CB of $GdCrO_3$ are active substance for photocatalytic reduction of NO_3^- when formic acid was used as hole scavenger. Meanwhile, Pd nanoparticles not only enhanced the photocatalytic efficiency but also improved the selectivity of 1 wt%Pd/$GdCrO_3$.

Due to the modification of Pd, the photocatalytic reduction of nitrate over 1 wt% Pd/$GdCrO_3$ was different from $GdCrO_3$. As shown in Fig. 8, $GdCrO_3$ is photoactivated and electron-hole pairs are photogenerated under UV illumination (Eq. (8)). These photo-generated electrons would immigrate to the conduction band of $GdCrO_3$ and then be entrapped by the Pd loaded on $GdCrO_3$ because of the strong electron-sink effect of Pd nanoparticles, which could delay the recombination of charge carriers effectively. The photo-generated electrons and holes were then consumed by nitrate and formic acid, respectively. The $CO_2 \cdot -$ radical could be produced during the reaction of photo-generated holes and formic anions (Eq. (9)). On one hand, there is no concern over $\cdot OH$ radical formation for $GdCrO_3$ due to the impossibility of water oxidation at lower potential of 0.68 V for VBM. On the other hand, EPR of $GdCrO_3$ composite also indicated that there was no $\cdot OH$ radicals production (Fig. 7b). Since $CO_2 \cdot -$ radicals could be produced by both photogenerated hole and $\cdot OH$ radicals reacting with formic acid, no $\cdot OH$ radicals generation during the photoreduction process also confirmed that photogenerated hole of $GdCrO_3$ reacted with formic acid to produce $CO_2 \cdot -$ radicals. Both $CO_2 \cdot -$ radicals (E° = -1.8 V) and e- cb (E° = -2.02 V) have strong reductive ability to reduce nitrate [E°(NO_3^- NO_3^- / NO_2^-) = 0.94 V), E°(NO_3^-/ NH_4^+) = 1.203 V), E°(NO_3^-/N_2) = 1.25 V)] (Eqs. (10)–(14)) and nitrite [E°(NO_2^- NO_2^- / NH_4^+ $NH+$ 4) = 0.897 V), E°(NO_2^- NO_2^- /N_2) = 1.45) (Eqs. (15)–(17)) [18,34,47,67]. Nitrate photocatalytic reduction proceeded step-wise and the conversion of nitrate into nitrite
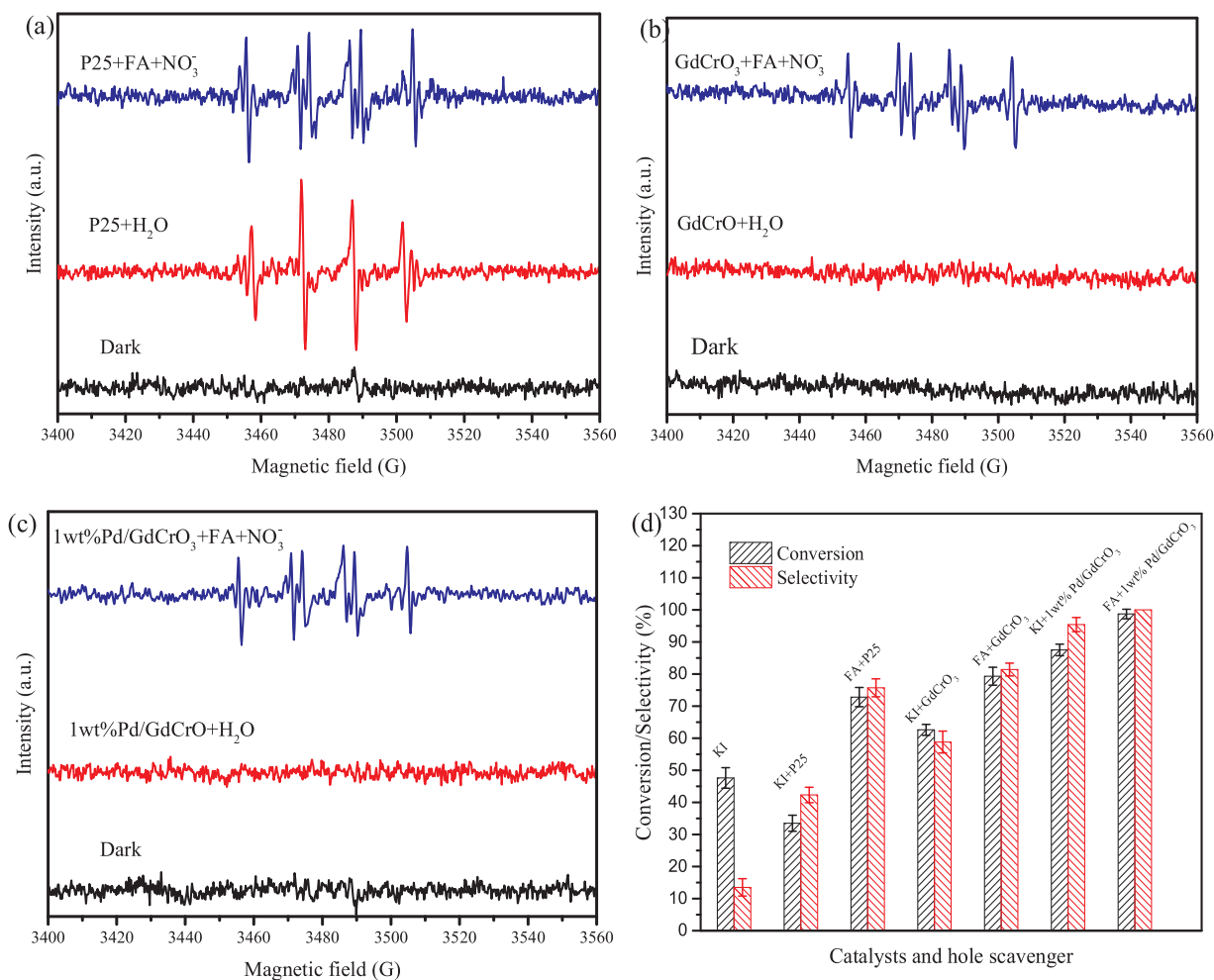
Fig. 7. Detection of EPR signals in different system (a–c); Nitrate conversion and N₂ selectivity over different photocatalysts in the present of hole scavenger (d).

mainly occurred within 20 min. And then the concentration of nitrite rapidly decreased with the reaction time (Fig. 5c), While NH+ 4 was maintained at a low level. Thus, we suggested that nitrite was selectively reduced to N₂ by photo-generated electrons under the promotion of Pd nanoparticles (Eq. (16)). As described in Section 3.3, NO – 2 was reduced to NO* on the Pd surface, followed by a decomposition step to N* and O* (an adsorbate on Pd is denoted using an asterisk). Then the reduction of NO – 2 in the vicinity of the N* could yield N₂O* which
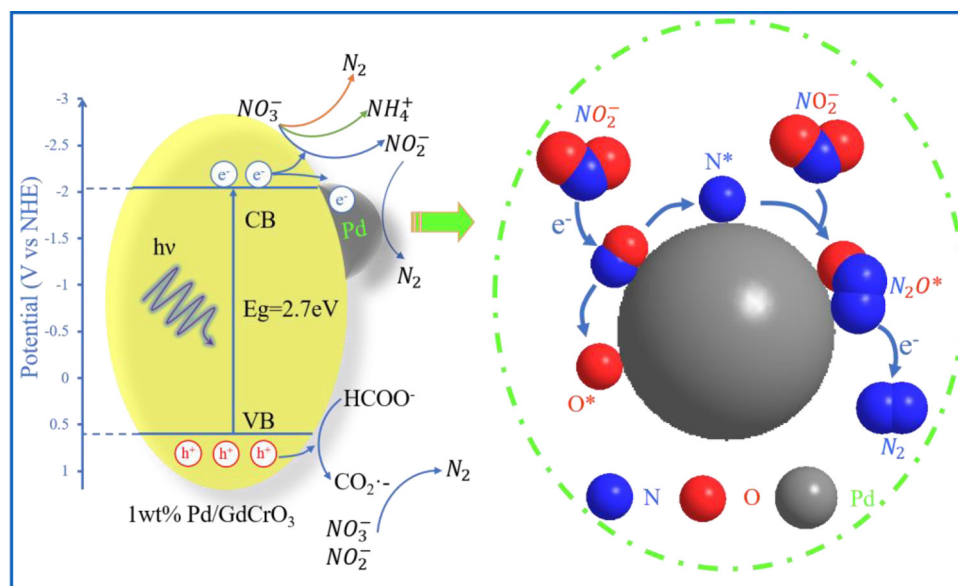

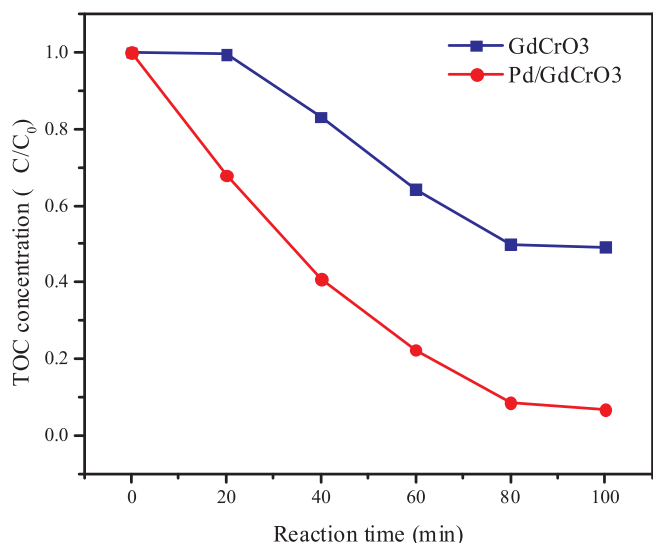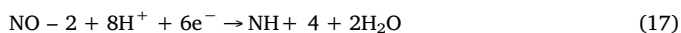**Fig. 8.** The proposed photocatalytic mechanisms of 1 wt% Pd/GdCrO₃ for photocatalytic reduction of nitrate.

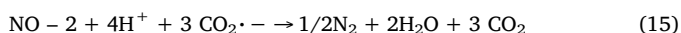**Fig. 9.** Time course of TOC during the process of photocatalytic reduction of nitrate.

would be preferentially transformed into N_2. Thus, high concentration of NO – 2 enhanced the likelihood of N* encountering NO – 2, resulting in increase of N_2 selectivity.

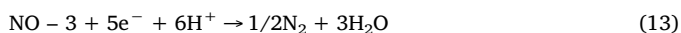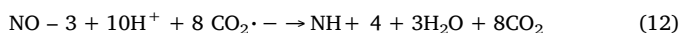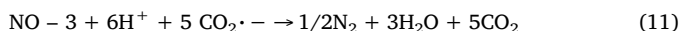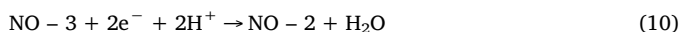$$GdCrO_3 + h\nu \rightarrow e^- + h^+ \tag{8}$$

$$HCOO^- + h^+ \rightarrow H^+ + CO_2 \cdot - \tag{9}$$

$$NO - 3 + 2e^- + 2H^+ \rightarrow NO - 2 + H_2O \tag{10}$$

$$NO - 3 + 6H^+ + 5\ CO_2 \cdot - \rightarrow 1/2N_2 + 3H_2O + 5CO_2 \tag{11}$$

$$NO - 3 + 10H^+ + 8\ CO_2 \cdot - \rightarrow NH + 4 + 3H_2O + 8CO_2 \tag{12}$$

$$NO - 3 + 5e^- + 6H^+ \rightarrow 1/2N_2 + 3H_2O \tag{13}$$

$$NO - 3 + 8e^- + 10H^+ \rightarrow NH + 4 + 3H_2O \tag{14}$$

$$NO - 2 + 4H^+ + 3\ CO_2 \cdot - \rightarrow 1/2N_2 + 2H_2O + 3\ CO_2 \tag{15}$$

$$NO_2^- + 4H^+ + 3e^- \xrightarrow{Pd} 1/2N_2 + 2H_2O \tag{16}$$

$$NO - 2 + 8H^+ + 6e^- \rightarrow NH + 4 + 2H_2O \tag{17}$$
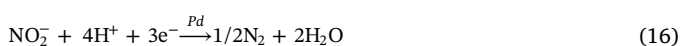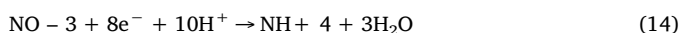
Since the photocatalytic reduction of nitrate was mainly by $CO_2 \cdot -$ and e- cb, the e- cb would play the dominant role when KI was used as the hole scavenger. Thus, compared with 1 wt% Pd/GdCrO₃, both the photocatalytic efficiency and N_2 selectivity of GdCrO₃ decreased more obviously as KI was added in. In addition, although addition of hole scavenger (formic acid) could improve the removal efficiency of nitrate and selectivity, the residual formic acid was undesired during the water treatment process. Therefore, we further evaluate the variation of TOC of formic acid during the photocatalytic reduction of nitrate process (Fig. 9). The removal of TOC was more effective by using 1 wt% Pd/GdCrO₃ than by using GdCrO₃, which was also in accordance to the photocatalytic reduction rate of nitrate. Since there were less than 7% TOC left after 100 min photocatalytic reaction over 1 wt%Pd/GdCrO₃, the problem of residual formic acid could be well resolved by prolonging the reaction time or adjusting the stoichiometric ratio of formic acid.

4. Conclusions

Pd/GdCrO₃ composite with high photocatalytic reduction efficiency of nitrate and selectivity to N_2 was successfully synthesized by solid state combustion and photodeposition methods. Due to the negative conduction band value of GdCrO₃ and co-catalyst effect of Pd, 1 wt%

Pd/GdCrO₃ showed high photocatalytic activity for nitrate conversion (98.7%) and N_2 selectivity (100%). Even after six cycling runs, 1 wt% Pd/GdCrO₃ could still remain high photocatalytic reduction rate of nitrate and selectivity to N_2. Notably, The co-catalyst Pd not only improved the utilization of charge carriers of GdCrO₃ so as to enhancing the photocatalytic activity, but also promoted the transformation of the initially accumulated NO – 2 to N_2 (NO – 2 → NO* → N* + O*, N* + NO – 2 → N₂O* → N₂). Furthermore, different from P25, both photogenerated electrons and $CO_2 \cdot^-$ played important role in photocatalytic reduction process. Thus, this study provided a simple and efficient way to improve the photocatalytic activity and selectivity to N_2, which might be beneficial to the environment remediation and water purification processes.

Appendix A. Supplementary data

Supplementary material related to this article can be found, in the online version, at doi:https://doi.org/10.1016/j.apcatb.2018.03.055.

References

[1] J.F. Power, J.S. Schepers, Agric. Ecosyst. Environ. 26 (1989) 165–187.
[2] F.T. Wakida, D.N. Lerner, Water Res. 39 (2005) 3–16.
[3] L. Knobeloch, B. Salna, A. Hogan, J. Postle, H. Anderson, Environ. Health Perspect. 108 (2000) 675–678.
[4] B. Bems, F.C. Jentoft, R. Schlögl, Appl. Catal. B Environ. 20 (1999) 155–163.
[5] Q. Guo, C. Zhou, Z. Ma, Z. Ren, H. Fan, X. Yang, Chem. Soc. Rev. 45 (2016) 3701–3730.
[6] L. Jing, W. Zhou, G. Tian, H. Fu, Chem. Soc. Rev. 42 (2013) 9509–9549.
[7] M. Ge, C. Cao, J. Huang, S. Li, Z. Chen, K.-Q. Zhang, S.S. Al-Deyab, Y. Lai, J. Mater. Chem. A 4 (2016) 6772–6801.
[8] H. Xu, S. Ouyang, L. Liu, P. Reunchan, N. Umezawa, J. Ye, J. Mater. Chem. A 2 (2014) 12642.
[9] Z. Zhang, S.-W. Cao, Y. Liao, C. Xue, Appl. Catal. B Environ. 162 (2015) 204–209.
[10] D.B. Ingram, S. Linic, J. Am. Chem. Soc. 133 (2011) 5202–5205.
[11] X. Wei, C. Shao, X. Li, N. Lu, K. Wang, Z. Zhang, Y. Liu, Nanoscale 8 (2016) 11034–11043.
[12] Y. Yang, J. Wen, J. Wei, R. Xiong, J. Shi, C. Pan, ACS Appl. Mater. Interface 5 (2013) 6201–6207.
[13] P. Chen, F. Wang, Z.-F. Chen, Q. Zhang, Y. Su, L. Shen, K. Yao, Y. Liu, Z. Cai, W. Lv, G. Liu, Appl. Catal. B Environ. 204 (2017) 250–259.
[14] X. Liu, Z. Xing, Y. Zhang, Z. Li, X. Wu, S. Tan, X. Yu, Q. Zhu, W. Zhou, Appl. Catal. B Environ. 201 (2017) 119–127.
[15] J. Pan, Y. Sheng, J. Zhang, J. Wei, P. Huang, X. Zhang, B. Feng, J. Mater. Chem. A 2 (2014) 18082–18086.
[16] R. Zhang, X. Wang, J. Song, Y. Si, X. Zhuang, J. Yu, B. Ding, J. Mater. Chem. A 3 (2015) 22136–22144.
[17] E. Grabowska, J. Reszczynska, A. Zaleska, Water Res. 46 (2012) 5453–5471.
[18] F. Zhang, R. Jin, J. Chen, C. Shao, W. Gao, L. Li, N. Guan, J. Catal. 232 (2005) 424–431.
[19] J. Sá, C.A. Agüera, S. Gross, J.A. Anderson, Appl. Catal. B Environ. 85 (2009) 192–200.
[20] G. Liu, S. You, M. Ma, H. Huang, N. Ren, Environ. Sci. Technol. 50 (2016) 11218–11225.
[21] L. Li, Z. Xu, F. Liu, Y. Shao, J. Wang, H. Wan, S. Zheng, J. Photochem. Photobiol., A 212 (2010) 113–121.
[22] Z.Q. Lin, S.J. Yuan, W.W. Li, J.J. Chen, G.P. Sheng, H.Q. Yu, Water Res. 109 (2017) 88–93.
[23] R. Lucchetti, L. Onotri, L. Clarizia, F.D. Natale, I.D. Somma, R. Andreozzi, R. Marotta, Appl. Catal. B Environ. 202 (2017) 539–549.
[24] Dd.B. Luiz, S.L.F. Andersen, C. Berger, H.J. José, Rd.F.P.M. Moreira, J. Photochem. Photobiol. A 246 (2012) 36–44.
[25] H. Adamu, A.J. McCue, R.S.F. Taylor, H.G. Manyar, J.A. Anderson, Appl. Catal. B Environ. 217 (2017) 181–191.
[26] J. Hirayama, Y. Kamiya, ACS Catal. 4 (2014) 2207–2215.
[27] Hiroshi Kominami a, Akitoshi Furusho a, Shin-ya Murakami a, Hiroyuki Inoue a,

Yoshiya Kera a and Bunsho Ohtani b, Catal. Lett., (2001).

[28] H. Kominami, T. Nakaseko, Y. Shimada, A. Furusho, H. Inoue, S.Y. Murakami, Y. Kera, B. Ohtani, Chem. Commun. (Camb.) (2005) 2933–2935.
[29] J.A. Anderson, Catal. Today 175 (2011) 316–321.
[30] J.A. Anderson, Catal. Today 181 (2012) 171–176.
[31] H.-T. Ren, S.-Y. Jia, J.-J. Zou, S.-H. Wu, X. Han, Appl. Catal. B Environ. 176-177 (2015) 53–61.
[32] O.S.G.P. Soares, M.F.R. Pereira, J.J.M. Órfão, J.L. Faria, C.G. Silva, Chem. Eng. J. 251 (2014) 123–130.
[33] N. Wehbe, M. Jaafar, C. Guillard, J.-M. Herrmann, S. Miachon, E. Puzenat, N. Guilhaume, Appl. Catal. A Gen. 368 (2009) 1–8.
[34] J. Hirayama, H. Kondo, Y.-k. Miura, R. Abe, Y. Kamiya, Catal. Commun. 20 (2012) 99–102.
[35] S. Chu, Y. Wang, Y. Guo, J. Feng, C. Wang, W. Luo, X. Fan, Z. Zou, ACS Catal. 3 (2013) 912–919.
[36] M. Shand, J.A. Anderson, Catal. Sci. Technol. 3 (2013) 879.
[37] J. Sá, T. Berger, K. Föttinger, A. Riss, J.A. Anderson, H. Vinek, J. Catal. 234 (2005) 282–291.
[38] Y.F. Sittinun Tawkaew, Sku Yin, Tsugio Sato, Colloids Surf. A (2001).
[39] J.M. Slocik, A.O. Govorov, R.R. Naik, Angew. Chem. Int. Ed. Engl. 47 (2008) 5335–5339.
[40] O. Hamanoi, A. Kudo, Chem. Lett. 31 (2002) 838–839.
[41] A. Kudo, K. Domen, K.-i. Maruya, T. Onishi, J. Catal. 135 (1992) 300–303.
[42] G.N.P. Oliveira, P. Machado, A.L. Pires, A.M. Pereira, J.P. Araújo, A.M.L. Lopes, J. Phys. Chem. Solids 91 (2016) 182–188.
[43] M. Kaiser, J. Alloys Compd. 719 (2017) 446–454.
[44] K.M. Parida, A. Nashim, S.K. Mahanta, Dalton Trans. 40 (2011) 12839–12845.
[45] S. Jung, S. Bae, W. Lee, Environ. Sci. Technol. 48 (2014) 9651–9658.
[46] O.S.G.P. Soares, J.J.M. Órfão, M.F.R. Pereira, Appl. Catal. B Environ. 102 (2011) 424–432.
[47] W. Gao, R. Jin, J. Chen, X. Guan, H. Zeng, F. Zhang, N. Guan, Catal. Today 90 (2004) 331–336.
[48] Y.-N. Kim, M.Y. Kim, M. Choi, Chem. Eng. J. 289 (2016) 423–432.
[49] Z. Gao, Y. Zhang, D. Li, C.J. Werth, Y. Zhang, X. Zhou, J. Hazard. Mater. 286 (2015) 425–431.
[50] S.T. Kochuveedu, Y.H. Jang, D.H. Kim, Chem. Soc. Rev. 42 (2013) 8467–8493.
[51] M.J. Kale, T. Avanesian, P. Christopher, ACS Catal. 4 (2014) 116–128.
[52] K. Doudrick, T. Yang, K. Hristovski, P. Westerhoff, Appl. Catal. B Environ. 136-137 (2013) 40–47.
[53] K. Yoshii, J. Solid State Chem. 159 (2001) 204–208.
[54] N. Zhang, S. Xie, B. Weng, Y.J. Xu, J. Mater. Chem. A 4 (2016) 18804–18814.
[55] X. Bai, R. Zong, C. Li, D. Liu, Y. Liu, Y. Zhu, Appl. Catal. B: Environ. 147 (2014) 82–91.
[56] L. Kavan, M. Gra1tzel, S.E. Gilbert, C. Klemenz, H.J. Scheel, J. Am. Chem. Soc. 118 (1996) 6716–6723.
[57] Y.J. Hao, B. Liu, L.G. Tian, F.T. Li, J. Ren, S.J. Liu, Y. Liu, J. Zhao, X.J. Wang, ACS. Appl. Mater. Interface 9 (2017) 12687–12693.
[58] F.T. Li, Y.L. Li, M.J. Chai, B. Li, Y.J. Hao, X.J. Wang, R.H. Liu, Catal. Sci. Technol. 6 (2016) 7985–7995.
[59] P. Zhang, T. Wang, X. Chang, J. Gong, Acc. Chem. Res. 49 (2016) 911–921.
[60] R. Marschall, Adv. Funct. Mater. 24 (2014) 2421–2440.
[61] D. Shuai, J.K. Choe, J.R. Shapley, C.J. Werth, Environ. Sci. Technol. 46 (2012) 2847–2855.
[62] Y. Wang, J. Liu, P. Wang, C.J. Werth, T.J. Strathmann, ACS Catal. 4 (2014) 3551–3559.
[63] H. Shin, S. Jung, S. Bae, W. Lee, H. Kim, Environ. Sci. Technol. 48 (2014) 12768–12774.
[64] W.H. Koppenol, J.D. Rush, J. Phys. Chem. 91 (1987) 4429–4430.
[65] M.A.B. Laura L. Perissinotti, and Marı´a A. Grela*, Langmuir, (2001).
[66] H.O. Tugaoen, S. Garcia-Segura, K. Hristovski, P. Westerhoff, Sci. Total Environ. 599-600 (2017) 1524–1551.
[67] R. Jin, W. Gao, J. Chen, H. Zeng, F. Zhang, Z. Liu, N. Guan, J. Photochem. Photobiol. A 162 (2004) 585–590.